Ultramicroscopy 218 (2020) 113093

Contents lists available at ScienceDirect

Ultramicroscopy

journal homepage: www.elsevier.com/locate/ultramic

Approximant-based orientation determination of quasicrystals using electron backscatter diffraction

Grzegorz Cios*[a], Gert Nolze[b,c], Aimo Winkelmann[a,g], Tomasz Tokarski[a], Ralf Hielscher[d], Radoslaw Strzałka[e], Ireneusz Bugański[e], Janusz Wolny[e], Piotr Bała[f,a]

[a] Academic Centre for Materials and Nanotechnology, AGH University of Science and Technology, al. A. Mickiewicza 30, Krakow 30-059, Poland
[b] Federal Institute for Materials, Research and Testing (BAM), Unter den Eichen 87, Berlin 12205, Germany
[c] TU Bergakademie Freiberg, Institute for Mineralogy, Brennhausgasse 14, Freiberg, 09596 Germany
[d] Technical University Chemnitz, Department of Mathematics, Reichenhainer Straße 39, Chemnitz 09126, Germany
[e] Faculty of Physics and Applied Computer Science, AGH University of Science and Technology, al. A. Mickiewicza 30, 30-059 Krakow, Poland
[f] Faculty of Metals and Industrial Computer Science, AGH University of Science and Technology, al. A. Mickiewicza 30, Krakow 30-059, Poland
[g] Department of Physics, SUPA, University of Strathclyde, Glasgow G4 0NG, United Kingdom

ARTICLE INFO

Keywords:
EBSD
Quasicrystal
Approximant
Crystal orientation
Data processing,

ABSTRACT

Orientation mapping of quasicrystalline materials is demonstrated using crystalline approximant structures in the technique of electron backscatter diffraction (EBSD). The approximant-based orientations are symmetrised according to the rotational point group of the quasicrystal, including the visualization of orientation maps using proper colour keys for quasicrystal symmetries. Alternatively, approximant-based orientation data can also be treated using pseudosymmetry post-processing options in the EBSD system software, which enables basic grain size estimations. Approximant-based orientation analyses are demonstrated for icosahedral and decagonal quasicrystals.

1. Introduction

Since the discovery of a “metallic phase with long-range orientational order and no translational symmetry” in 1982 [1], quasicrystals (QC) [2] remain an extremely fascinating topic in materials science [3]. Applications of quasicrystalline materials include, for example, the strengthening of alloys with quasicrystalline particles in alloys of aluminium [4–8] and magnesium [9,10]. It was also observed that quasicrystals can show a higher hydrogen uptake than conventional hydrogen storage materials [11]. Quasicrystals are known for their high wear resistance and low friction coefficient [12]. One peculiar application of quasicrystals were non-sticky coatings deposited on frying pans [13,14].

The crystal structure of a quasicrystal is characterised by a non-periodic arrangement of atoms, which no longer complies with three-dimensional translation symmetry as a prerequisite of the classical space-group types [15]. Therefore, it can become a challenge to characterise quasicrystalline materials if the available analysis methods do not allow for quasicrystal symmetry. In scanning electron microscopy, this includes common crystallographic techniques in materials science, such as electron backscatter diffraction (EBSD) [16,17] or transmission Kikuchi diffraction (TKD) [18]. EBSD and TKD are both based on the detection of Kikuchi diffraction patterns [19,20], which carry the crystallographic information from the sample.

In order to facilitate the application of EBSD to quasicrystalline materials, we discuss two examples, namely an icosahedral quasicrystalline material obtained after rapid solidification and decagonal quasicrystals from a crystal growth experiment.

Icosahedral phases are the only known quasicrystals with 3D quasiperiodicity. Decagonal quasicrystals are the largest family of axial QC with 2D quasiperiodicity. The latter commonly represent a sequence of 2, 4, 6 or 8 quasiperiodic layers periodically stacked along the 10-fold axis [21]. The bonds within layers can be as strong as of those between layers which results in atomic shifts of several tenths of angstrom out of the layers. Beside these misalignments the layer stacking appears strictly periodic, which is concluded from X-ray or electron diffraction patterns. From the strong diffuse scattering for lattice planes perpendicular to the 10-fold axis on the other hand the missing or only partial periodicity within the layers was deduced. A consequence of the atomic structure of the discussed quasicrystals is the appearance of additional 5-fold and 10-fold rotational symmetry in their Kikuchi diffraction patterns, as is shown in Fig. 1.

* Corresponding author.
E-mail address: Ciosu@agh.edu.pl (G. Cios).

https://doi.org/10.1016/j.ultramic.2020.113093
Received 15 April 2020; Received in revised form 28 July 2020; Accepted 9 August 2020
Available online 14 August 2020

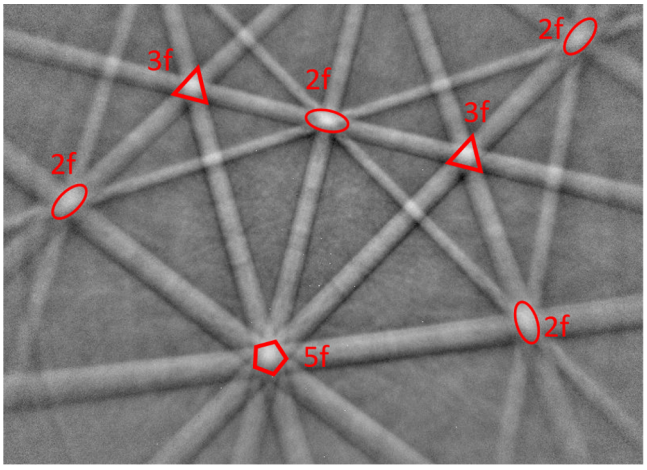

(a)

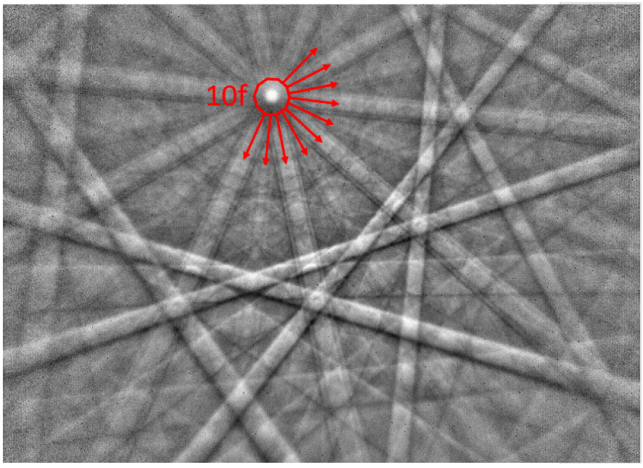

(b)

Fig. 1. Kikuchi patterns observed in EBSD measurements with marked typical symmetry elements of (a) the icosahedral and (b) the decagonal quasicrystalline structures.

Despite that fact that these quasicrystalline materials can show clear Kikuchi diffraction (BKD) patterns, there is a lack of dedicated analysis options for quasicrystal orientation determinination and phase discrimination in the commercial EBSD systems. This is why, so far, the applications of EBSD to quasicrystals were mainly limited to the analysis of individual BKD patterns [22–31]. The orientation mapping of quasicrystals in a Mg alloy was demonstrated in [32], but the EBSD patterns recorded from different grains were still analysed individually due to a lack of software integration. Using dedicated software for dictionary-based indexing [33], orientation determination was demonstrated for a quasicrystalline microstructure in [34].

One approach to take into account the unconventional point group symmetries in the orientation analysis of quasicrystal Kikuchi patterns is to consider crystal structures which produce closely similar Kikuchi diffraction patterns but which can be described by a three-dimensionally periodic lattice, the so-called approximants. In the context of pseudosymmetry misindexing problems in EBSD system software, the close structural relationship of the cubic approximant crystal structure of α-Al(Fe,Mn,Cr)Si to that of the corresponding icosahedral quasicrystal was discussed in [35]. From a different perspective, this observation points to a possibility for the analysis of quasicrystals via their approximant structures. Because the approximant is a conventional crystal structure, it can be imported into the available EBSD system software and used for indexing of quasicrystal EBSD data, provided that the extra symmetry of the quasicrystal structure is taken into account accordingly in the data treatment.

Table 1
Overview of quasicrystalline symmetries and available approximants suitable for an orientation description. The crystal structure data is given in the respective Table in the Appendix (other approximant are discussed in [21]).

Symmetry	QC Point Group	Approximant	Approx. Point Group	Table	Ref.
Octagonal	8/mmm	β-Mn/$Mn_{12}Si_5$	4/m	A.1	[37]
Decagonal	10/mmm	$Al_{13}Co_4$	m	A.2	[38]
Dodecagonal	12/mmm	Mn_4Si	6/mmm	A.3	[39]
Icosahedral	-5 -3 2/m	W-TiZrNi	m -3	A.4	[40]

Based on the similarities between quasicrystals and their approximant structures, we demonstrate orientation determination from quasicrystal Kikuchi patterns using approximant structures in commercial EBSD systems and we discuss various data treatment possibilities to transform approximant orientation data into approximated quasicrystalline orientation data.

2. Materials and methods

2.1. EBSD Orientation analysis using approximants

In Table 1, we list possible known approximant structures for use in EBSD systems. The approximant structures have a lower symmetry than the corresponding quasicrystal. As a result, when orientations are determined based on the approximant crystal symmetry, the EBSD system can assign symmetrically non-equivalent approximant orientations to quasicrystal Kikuchi patterns which actually represent equivalent quasicrystal orientations. For the often used IPF-map color visualization [36], this means that points in a common quasicrystal grain can show different colors when indexed with the approximant structure. The potential assignment of seemingly different orientations within a grain will influence the grain detection, if the actual equivalence of these orientations in the higher symmetry point group of the quasicrystal cannot be accounted for by the EBSD analysis software.

To circumvent this problem in a first approximation, post-processing of the approximant orientation data can be applied completely inside the EBSD system software using functionality that is commonly used for cleaning of pseudosymmetry issues [41]. As will be discussed below, this provides a relatively simple solution for problems like grain size estimations of quasicrystalline materials without additional dedicated software. While the grain detection by itself could potentially also be achieved by a statistical similarity analysis of the backscattered Kikuchi patterns [42–45], the indexing by an approximant structure does provide quantitative orientation data. The key problem, however, is that the further analysis of this orientation data by the EBSD system software is limited in terms of correct visualization and quantititive analysis of genuine quasicrystal orientations. For example, the symmetry properties of orientations in quasicrystal point groups are neglected in the available IPF color keys. In effect, even if we can assign a uniform color to specific grains using the pseudosymmetry cleaning, it can still be hard to recognize which other grains actually correspond to nearly equivalent orientations of the quasicrystal when using the approximant IPF color key. A possible option to incorporate the symmetry of the quasicrystal into the orientation data therefore is to index the data using an approximant structure in the EBSD system software as discussed above, and then use dedicated external software to symmetrize the approximant-based orientation data according to the correct quasicrystal point group. This will be described below using the open source software MTEX [46].

2.2. Materials investigated

As the basic starting material for the icosahedral quasicrystal, an

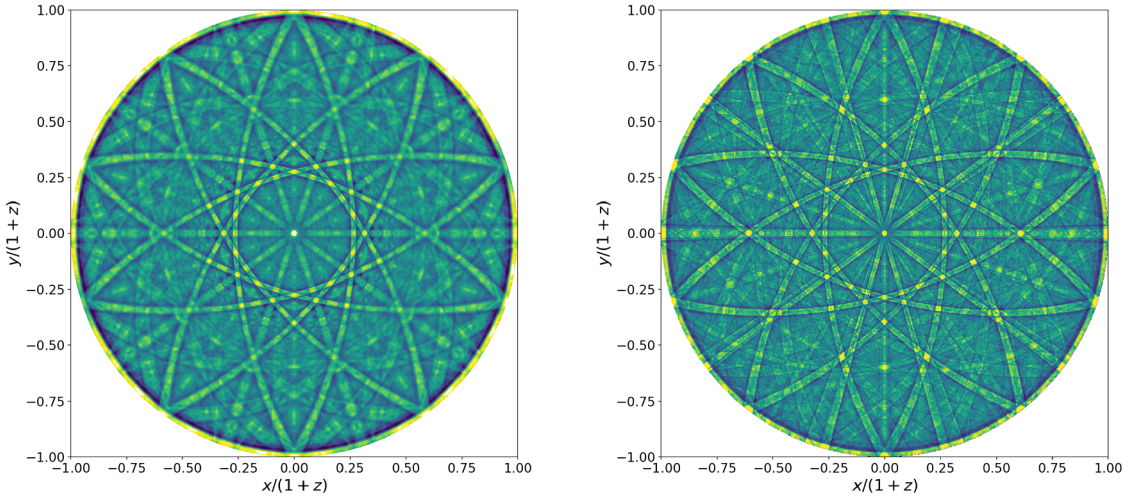

(a) AlNiCo (b) $Al_{13}Co_4$

Fig. 2. Hemispherical diffraction signals displayed in stereographic projection. (a) experimental BKD signal of the decagonal AlNiCo, (b) simulated signal of the monoclinic approximant structure $Al_{13}Co_4$ using the dynamical theory of electron diffraction [54].

alloy of Ti40Zr40Ni20 was arc melted in high vacuum evacuated argon atmosphere from high-purity elements using an Arc Melter AM (Edmund Bühler GmbH). The solid sample was produced by suction casting into a copper mould of $\varnothing = 6$ mm and a length of 55 mm. The chosen composition and casting technique are based on previous studies in [47]. The solidified cylinder was polycrystalline, with grains of icosahedral quasicrystalline symmetry. The EBSD analysis was performed on a cross-section with a normal direction referred to as Z-axis.

The AlCoNi decagonal quasicrystals were grown using the Czochralski method from Al-rich melts as described in [48].

2.3. Sample preparation

The sample surfaces were manually prepared using standard metallographic polishing techniques: grinding down to 2000 grit SiC paper followed by a polishing with 3 μm and 1 μm diamond suspension. The last step was a surface finishing by polishing for 10 min with colloidal silica (50 nm).

2.4. EBSD data acquisition

The decagonal and icosahedral quasicrystalline samples were investigated in a LEO 1530VP FE-SEM (Zeiss) and in a Versa 3D FE-SEM (FEI), both operated at 20 kV with a beam current of $\approx$ 11 nA.

For the orientation maps the EBSD patterns of the e$^-$Flash^{HR} detector (Bruker Nano) mounted on the LEO were binned down to a resolution of 160 × 115 pixels, whereas the patterns of the Hikari detector (EDAX) mounted on the Versa were binned down to an image size of 120 × 120 pixels. For subsequent post-processing, all raw patterns were stored. To indicate the quality of sample preparation, example BKD patterns are shown in Fig. 1.

2.5. EBSD data analysis

The different approaches for EBSD data analysis which we applied in the present study are summarized in the list below. For quick reference in the text, each method of data treatment will be referred to by the respective abbreviation in brackets.

a) Hough transform (HT) based indexing was carried out using the approximant structures in Bruker Esprit 1.94 (Bruker Nano GmbH, Berlin, Germany) and EDAX Team 4.5 (EDAX Inc., Mahwah, NJ, USA). This resulted in the raw approximant orientation data sets from the system software (HT-RAW), which were then treated by pseudosymmetry cleaning in EDAX OIM Analysis 7 or Oxford Instruments Channel5 (HT-PS) and subsequently symmetrized to the QC point group using MTEX (HT-MTEX)
b) In order to analyze the precision of the HT based approaches, pattern matching using dynamically simulated approximant data (PM-AP) was applied on the stored EBSD patterns [49–51]. See supplementary material for matched patterns.
c) For a comparison to true QC Kikuchi data, pattern matching was also carried out using experimental Kikuchi reference patterns [52] of the relevant quasicrystals (PM-QC)

3. Results

3.1. 2D quasiperiodicity

For phases with a quasicrystal symmetry $M/m\,m\,m$ ($M = 8, 10, 12$) and the respective enantiomorphic group $M\,2\,2$, the assignment of a quasicrystal orientation from an approximant orientation is possible based on the general discussion of Euler angles in [53]. For a non-rotated crystal with Euler angles $\{\psi, \theta, \varphi\} = \{0, 0, 0\}$ with the relevant pseudo-M-fold axis of the approximant along the Z-axis and aligned parallel to the M-fold axis of the quasicrystal, φ and θ of the approximant orientation can be directly used for the quasicrystal. The different multiplicity M can be accounted for by a correction of the Euler angle ψ, which describes a rotation around the main symmetry axis. If we call the determined angle of the approximant ψ^a, the corresponding equivalent Euler angles ψ^q of the quasicrystal are:

$$\psi^q = \psi^a \mod 360°/M \tag{1}$$

A given orientation derived within the point group of the approximant is thus related to a correspondingly higher number of orientation descriptions which are symmetry-equivalent in the point group of the quasicrystal.

As an example, we discuss the decagonal quasicrystal AlNiCo in combination with the monoclinic $Al_{13}Co_4$ as the approximant. The monoclinic axis of this approximant is the pseudo 10-fold axis. Fig. 2 compares the experimental Kikuchi diffraction signal of AlNiCo with a simulated intensity distribution [54] of the approximant.

The reference projection in Fig. 2(a) represents a symmetrized montage of several experimental Kikuchi diffraction patterns from the

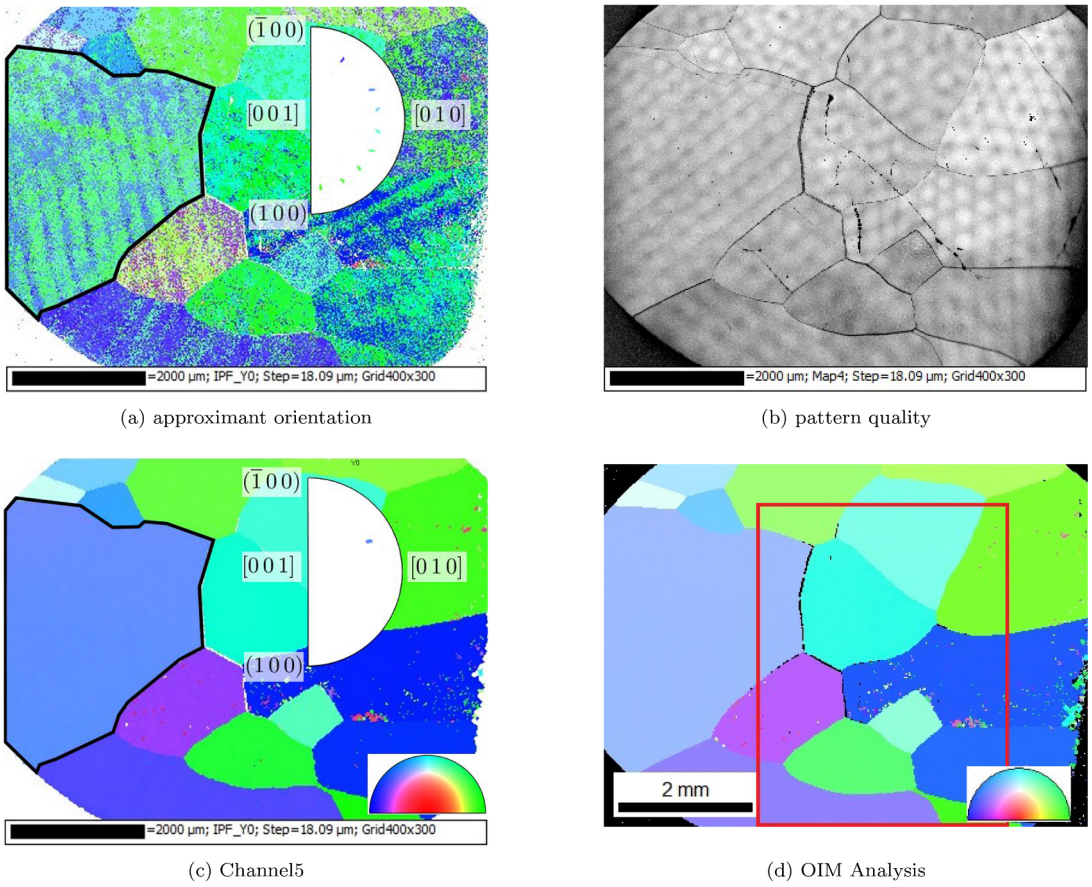

(a) approximant orientation

(b) pattern quality

(c) Channel5

(d) OIM Analysis

Fig. 3. IPF-Y map after indexing with the monoclinic approximant (a) (HT-RAW). The apparently systematic orientation selection in (a) is caused by the orientation-dependent variation in band detection at very low magnification visible as pattern quality in (b). After consideration of the five-fold rotation around [001], Channel5 (PS-HT) (c) and OIM Analysis (HT-PS) (d) recognise all grains correctly. The small colour deviations between (c) and (d) are the result of differently defined colour keys shown as inset. The red frame in (d) refers to the subset discussed in Fig. 4. (For interpretation of the references to colour in this figure legend, the reader is referred to the web version of this article.)

decagonal quasicrystal AlNiCo of point group $10/mmm$ [52]. For comparison, the simulated signal in Fig. 2(b) was calculated from the crystal structure data of $Al_{13}Co_4$. The monoclinic axis of the approximant is aligned with the 10-fold axis of the quasicrystal. The close similarity of the Kikuchi patterns in Fig. 2(a) and (b) illustrates that the approximant structure can be a suitable alternative to index actual quasicrystal Kikuchi patterns.

Using the approximant structure of $Al_{13}Co_4$ in the EBSD system software, we show the resulting orientation maps of the AlNiCo quasicrystal sample in Fig. 3(a). The visible speckling within grains in Fig. 3(a) indicates that the EBSD system is sensitive to effects of the lower symmetry of the approximant. We see different pseudosymmetric orientation solutions within the point group of the approximant, for the same quasicrystal orientation within a grain. If no specific pseudosymmetric solution would be preferred by the indexing algorithm of the EBSD system, each of the ten orientation solutions should be randomly distributed within a single grain. The grain marked on the left side of the map in Fig. 3(a), however, apparently displays only two different colours. The inverse pole figure inset for Y proves that this visual impression is misleading since the grain really contains 8 from possible 10 orientation descriptions. The missing two orientation solutions are possibly systematically rejected by the EBSD indexing algorithm due to a slightly higher mean angular deviation of the detected Kikuchi bands.

The systematic intra-grain features in Fig. 3(a) can also be seen in the pattern quality map in Fig. 3(b). These orientation artefacts are known to result from the change in projection center with changing position in the map, which systematically biases the orientation determination [55].

The initial, approximant-based EBSD orientation data shown in Fig. 3(a) would be of only limited value because the quasicrystal grains are highly influenced by the pseudosymmetric solutions of the approximant. In the following, we will discuss how this data can be corrected with the help of EBSD analysis software like Channel5 (Oxford Instruments) and OIM Analysis (EDAX) which contain options for pseudosymmetry cleaning of orientations. This functionality is applied for correction of the approximant orientations to result in a single symmetry-equivalent grain orientation for the quasicrystal. The number of equivalent orientation descriptions depends on the multiplicity M of the enantiomorphic symmetry and the point group of the approximant. In order to derive the orientation-consistent maps as in Fig. 3(c) and (d), the missing symmetries are additional rotations by multiples of 36 degrees around [001] which emulate the effect of an additional five-fold symmetry for the decagonal quasicrystal relative to the already existing two-fold symmetry of the approximant. This post-processing procedure results a correct recognition of grains, as can be seen by the uniform colors of the grains in Fig. 3(c) and (d).

While the grain sizes and shapes can be determined correctly by the approach discussed here, the interpretation of the actual grain colors in the orientation map is limited by the lower symmetry of the EBSD system color key for the point group $2/m$ of the approximant, which cannot convey the actual 10-fold symmetry. In order to obtain a correct colour coding for the quasicrystal orientations, we have used MTEX [46]. The IPF colour-coding considering the according enantiomorphic group 1 1 2 of the approximant is shown in Fig. 4(a). This colour coding

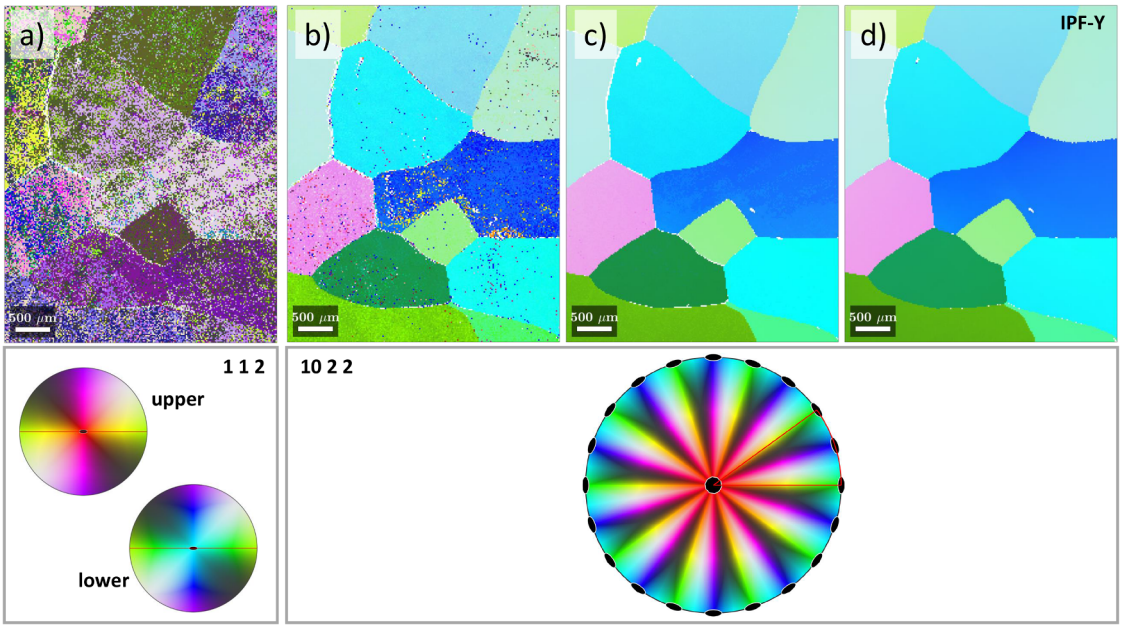

Fig. 4. IPF-Y orientation maps for decagonal AlNiCo. a) indexed with the $Al_{13}Co_4$ monoclinic approximant in the Bruker system software (Esprit 1.94) (HT-RAW) and displayed with a symmetry 1 1 2, b) MTEX-symmetrised orientations from a) for point group 10 2 2 (HT-MTEX), c) refined orientations from b) by pattern matching with dynamical simulation for $Al_{13}Co_4$ (PM-AP), d) pattern matching with experimental EBSD reference pattern using starting orientations from b) (PM-QC).

correctly describes orientations as composed of orientations only, in contrast to an ambiguous colour coding when using the Laue group $2/m$ [56]. The map in Fig. 4(a) covers the reduced region described by the red frame in Fig. 3(d) in order to allow a better discrimination of features.

For the consistent handling of orientation data from quasicrystals, MTEX makes it possible to freely define the relevant point groups and their colour keys based on rotation operators which are generators of these groups. Because the orientations of the approximant structure are a subgroup of the quasicrystal orientations, the approximant-based orientations can be symmetrized by the assignment of the quasicrystal point group to the approximant-based orientation data. This requires that the rotation axes are identically aligned, e.g. for 1 1 2 with $2 \| Z$ the 10-fold axis in 10 2 2 only need to be defined along Z. The two-fold axis $\perp 10$ can be defined e.g. to be along the X direction.

After processing of the orientation data shown in Fig. 4(a) by MTEX according to point group 10 2 2, the IPF map mostly shows a constant colour within the same grain, as seen in Fig. 4(b). In the symmetrized data, mainly some single pixels with different color remain, which we assign to indexing problems of the EBSD system software used during acquisition.

In Fig. 4(c), we have solved the misindexed points by a pattern matching approach using a dynamical Kikuchi pattern simulations as described in [49]. Caused by the lower symmetric approximant, some systematic orientation artefacts still remain, which are most visible in the blue grain which is in the right central part of the map. To further improve the orientation precision, we have also applied pattern matching against the experimental quasicrystal data as described in [52]. The corresponding orientation map is shown in Fig. 4(d).

The relative precision of the orientation data shown as the IPF-Y map in Fig. 4 can be estimated from the distribution of the Kernel average misorientation (KAM) angles, which we characterize by the value of the 95th percentile ϑ_{95} of the KAM angle distribution [55]. We found that the system software indexing results in $\vartheta_{95}^{(b)} = 1.6°$ (HT-MTEX). The approximant pattern matching leads to an improvement of this value to $\vartheta_{95}^{(c)} = 0.3°$ (PM-AP). For the pattern matching result using the experimental reference patterns as shown in Fig. 4(d), the 95th percentile of the KAM angle is reduced to $\vartheta_{95}^{(d)} = 0.12°$ (PM-QC), i.e. it is more than an order of magnitude better than for the initial result in Fig. 4(b). The significant difference between the approximant pattern matching result and the pattern matching to the experimental reference shows that the lower approximant symmetry is limiting the available orientation precision, i.e. approximant Kikuchi pattern simulations are less suitable for highest angular resolution analysis.

3.2. 3D quasiperiodicity

Quasicrystals with 3D periodicity, e.g. of icosahedral symmetry can be treated in the same way as the 2D quasicrystals discussed above, using subgroup relationships. To this end, it is useful to describe the orientation of the quasicrystal in such a way that it also fits the symmetry operators of the approximant. For an approximant with cubic symmetry $2/m\,\bar{3}$, the rotation axes of the quasicrystal should be oriented as shown in Fig. 5:

$$2 \| \ \vec{Z},$$
$$3 \| \ \vec{X} + \vec{Y} + \vec{Z},$$
$$5 \| \ \vec{X} + \vec{Y},$$

This setting of the icosahedral group is denoted as 2 3 5 [57] with $< 001 > - < 111 > - < 110 >$ as directions of view.

The gray-dotted cube indicates the main axes and represents one possibility to describe a cubic set of vertices as part of a pentagondodecahedron. From the remaining four other solutions of inserting a cube into the same pentagondodecahedron, one is given by red/blue lines. The two colours are used to indicate that there are two cubes with the same alignment but non-equivalent orientations. This cube cannot be transferred by rotations of the dodecahedron with the aim to change red to blue and blue to red.

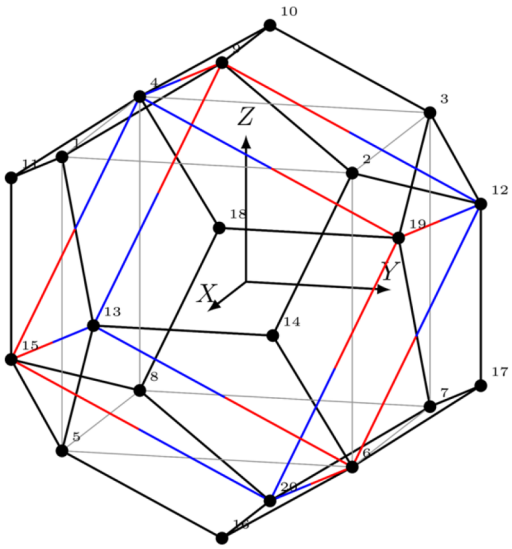

Fig. 5. Description of the orientation of a pentagonal dodecahedron by two differently oriented cubes. The gray-dotted cube has a symmetry of $m\bar{3}m$) and enables five solutions, whereas the blue-red coloured cube has a symmetry of $m\bar{3}$ and stands for ten possible orientation descriptions. (For interpretation of the references to colour in this figure legend, the reader is referred to the web version of this article.)

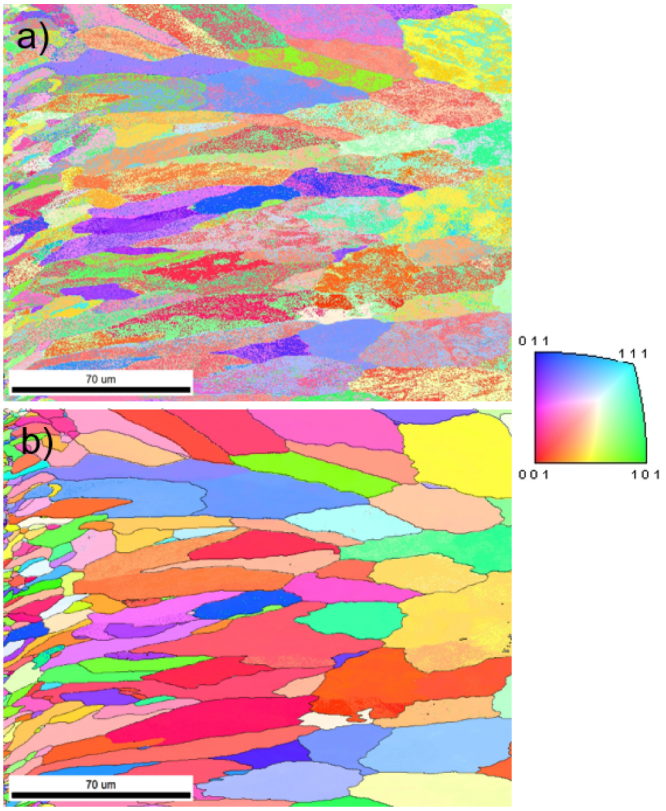

Fig. 6. Orientation determination of icosahedral quasicrystals by the cubic approximant W-TiZrNi. a) raw orientation data coloured for the sample normal (IPF-Z) (HT-RAW). b) result after pseudosymmetry cleaning using 72°rotations around $< 305 >$ in OIM Analysis (EDAX). Note: colouring uses the colour key for Laue group $m\bar{3}$ (bottom) because a 2 3 5 color key is not available in OIM Analysis (HT-PC).

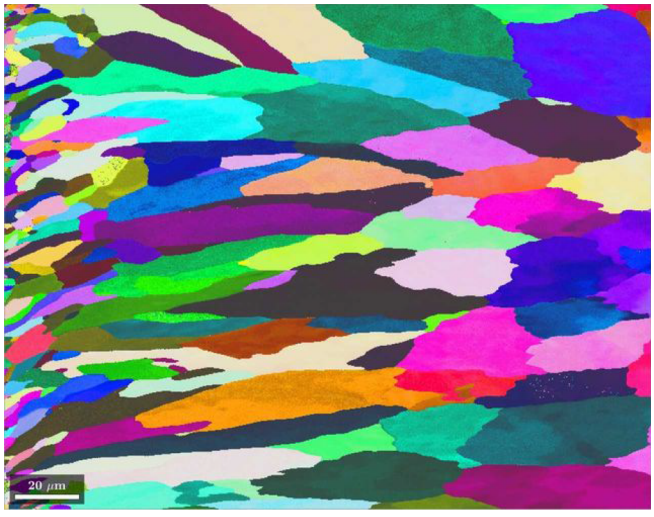

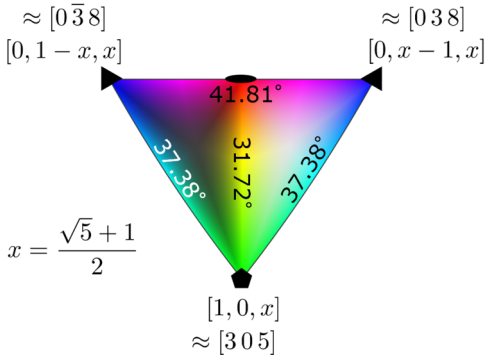

Fig. 7. Orientation mapping of icosahedral quasicrystals using raw orientation data derived from cubic approximants and symmetrization by MTEX. The colour key below for rotational group 2 3 5 is bounded by the five-fold, three-fold and two-fold axes, with their directions based on the golden ratio x [57] (HT-MTEX).

As for quasicrystals with 2D periodicity, the recognition of symmetry-equivalent orientations for a grain or misorientation computation requires the input of all missing symmetry-elements in the EBSD system software. Because of the higher symmetry this is more complicated. For instance, a five-fold rotation axis is also only roughly describable by a lattice direction since the exact rotation axis [1,0,x] with $x = (\sqrt{5} + 1)/2$ is 0.75°away from the low-indexed $< 305 >$. Similar conditions exist for the three-fold axis where some of them are parallel to $< 111 >$, the relevant alignment is, however, parallel to $[0, x - 1, x]$, see Fig. 7. Moreover, the correct description of the rotation axis in the system software is important since $< 305 >$ is not symmetry-equivalent to $< 503 >$.

In Fig. 6a, the orientation solution for the cubic approximant (W-TiZrNi, point group 23) is displayed.

Fig. 6 a shows the expected multiple orientation solutions within grains caused by the subgroup symmetry of the approximant. After manual implementation of the five-fold symmetry axis along $< 305 >$, all symmetry-equivalent orientation solutions are discovered and grains appear with a unique colour, cf. Fig. 6b. The colouring of the map, however, refers to the displayed colour key of the centrosymmetric group $m\bar{3}$ which is ambiguous for an evaluation of the crystal orientation [56]. However, for conclusions regarding grains or misorientations it is sufficient so that many investigations and

calculations can be performed.

We have defined the point group 2 3 5 in MTEX 5.2 and used this symmetry for plotting of orientation maps. Use of point group 2 3 5 extends the number of 12 symmetry-equivalent orientation descriptions for the symmetry group 2 3 to a number of 60 symmetry-equivalent orientation descriptions. In other words, MTEX checks each orientation whether one of the 60 descriptions practically matches to the orientation description found at the adjacent pixel. The resulting IPF-map is given in Fig. 7.

Note that the fundamental sector of the symmetry group 2 3 5 (below the map) is no more defined by lattice vectors of a three-dimensional periodic lattice, but by directions [*p, q, r*] based on the golden ratio *x*. There are low-indexed cubic lattice vectors close to these directions: [0-38], [038], and [305]. These directions can be often used since their angular deviations to the real directions are 0.35°and 0.75°which is in the order of the orientation precision and below the maximum misorientation used during grain detection.

3.3. Application to other crystal structures

The approach discussed here should work in any EBSD system software as long as it offers functionality which is required for the elimination of twin boundaries or for treatment of pseudosymmetry issues.

However, the symmetrisation procedure described above differs in the result from that used to correct pseudosymmetry issues as demonstrated in [58] using the example of pyrite (FeS_2, $m\bar{3}$). In [58], misindexed orientations were converted with respect to the higher symmetric group of $m\bar{3}m$ in order to ascribe a uniform orientation to a complete grain. The pseudo-symmetric solutions of pyrite were indeed different, however, and the correction procedure accounts for the limitations of the EBSD indexing software to detect a *lower* symmetry.

In contrast, for the quasicrystals discussed here, the problem is to index the *high* symmetry of the quasicrystal. For this type of "pseudosymmetry cleaning" [41], the different lower-symmetric orientation solutions of the approximant will be correctly assigned to a unique, symmetry-equivalent solution of the quasicrystal point group.

The approach used here should thus work in the same way for classical crystals of higher symmetry, for which only a lower symmetric structure description of a related phase is available. This is not uncommon for hexagonal phases, for which orthorhombic or monoclinic approximations in databases might be available.

4. Summary

In the study presented in this manuscript we used approximants to determine the crystal orientations of icosahedral and decagonal quasicrystalline samples by electron backscatter diffraction. We showed how some critical limitations of commercial EBSD software regarding the analysis of quasicrystals can be circumvented. We proposed to derive an approximate orientation of the quasicrystal from the orientation of a classical (periodic) crystalline phase, determined from a Kikuchi pattern of the quasicrystal, by symmetrization of the orientation data. We estimate that the resulting uncertainty for determining the quasicrystal orientation is similar to the uncertainty observed for conventional 3D-periodic crystals.

For orientation analyses of quasicrystalline materials with increased angular resolution, orientation data are sufficient as initial values for further orientation refinement. In contrast, dynamic pattern simulations of approximants do not provide reliable templates for high-precision orientation refinement, since orientation artefacts are introduced by the lower symmetry of the approximants and their patterns. In order to improve quasicrystal orientation precision, we have shown that experimental reference data can be used alternatively for the refinement of approximant-based quasi-crystalline orientations [52].

It is expected that similar procedures as demonstrated here for the icosahedral and decagonal quasicrystals can be applied to EBSD investigations of dodecagonal and octagonal quasicrystals and their approximants. In this way, the approach presented here facilitates the application of EBSD to quasicrystalline materials to study, among other topics, the rapid solidification and crystal growth of quasicrystalline phases.

Declaration of Competing Interest

The authors declare that they have no known competing financial interests or personal relationships that could have appeared to influence the work reported in this paper.

Acknowledgements

We would like to thank P. Gille (LMU, Munich) for providing the AlCoNi quasicrystal sample, and T. Kozieł (AGH-UST, Kraków) for providing the Ti40Zr40Ni20 alloy sample. We thank M. Buchheim and R. Saliwan-Neumann (BAM Berlin) for invaluable help with sample preparation and data collection, and K. Mehnert (ST Developments ApS) for analyzing the map displayed in fig. 3(c). This work was supported by the Polish National Agency for Academic Exchange (NAWA) grant no. PPI/APM/2018/1/00049/U/001 and no. PPN/ULM/2019/1/00068/U/00001. R.S., I.B. and J.W. kindly acknowledge support from National Science Center under grant no. 2019/33/B/ST3/02063.

Appendix A. Appendix

Table A.1
Crystal structure data of $Mn_{12}Si_5$ (Space-group type: no. 87 (I 4/m), a = 8.96 Å, c = 5.04 Å) octagonal quasicrystal approximant [37].

Atom	x	y	z	Occupation
Mn1	0.1169	0.1809	0.248	1
Mn2	0.0604	0.6339	0.0000	1
Si1	0.0869	0.6946	0.5000	1
Si2	0.0000	0.0000	0.0000	1

Table A.2
Crystal structure data of $Al_{13}Co_4$ (Space-group type: no. 8 (C m), a = 12.340 Å, b = 15.183 Å, c = 8.122 Å, $\alpha = 90°$, $\beta = 90°$, $\gamma = 108°$) decagonal quasicrystal approximant [38].

Atom	x	y	z	Occupation
Co1	0.3827	0.0863	0	1
Co2	0.3732	0.6045	0	1
Co3	0.0129	0.9094	0	1
Co4	0.018	0.5978	0	1
Co5	0.2774	0.3185	0.2925	1
Al1	0.1745	0.055	0	1
Al2	0.2803	0.3296	0	1
Al3	0.469	0.7675	0	1
Al4	0.424	0.923	0	0.3
Al5	0.031	0.7548	0	0.7
Al6	0.169	0.5224	0	1
Al7	0.4996	0.502	0	1
Al8	0.2307	0.702	0	1
Al9	0.212	0.9052	0	0.7
Al11	0.1119	0.1854	0.2176	1
Al12	0.1116	0.3641	0.2107	1
Al13	0.334	0.1769	0.2192	1
Al14	0.331	0.4919	0.2247	1
Al15	0.477	0.3678	0.2103	1
Al16	0	0.4985	0.2485	1
Al17	0.6171	0.9137	0	1
Al18	0.6269	0.3954	0	1
Al19	0.987	0.0903	0	1
Al20	0.982	0.402	0	1
Al21	0.7226	0.1827	0.2297	1
Al22	0.825	0.9455	0	1
Al23	0.72	0.6702	0	1
Al24	0.532	0.2329	0	1
Al25	0.576	0.077	0	0.3
Al26	0.966	0.2452	0	0.7
Al27	0.8313	0.447	0	1
Al28	0.7693	0.2975	0	1
Al29	0.788	0.095	0	0.7
Al30	0.888	0.3143	0.2826	1
Al31	0.8884	0.1241	0.2717	1
Al32	0.666	0.3226	0.2806	1
Al33	0.669	0.0087	0.2793	1
Al34	0.523	0.1219	0.2898	1

Table A.3
Crystal structure data of Mn_4Si (Space-group type: no. 191 (P 6/mmm), a = 17.058 Å, c = 4.64Å) dodecagonal quasicrystal approximant [39].

Atom	x	y	z	Occupation
Si1	0.0000	0.0000	0.2671	0.34
Mn1	0.0000	0.0000	0.2671	0.64
Mn2	0.2680	0.0000	0.2557	1
Mn3	0.5778	0.1555	0.2457	1
Mn4	0.1349	0.0000	0.0000	1
Mn5	0.2784	0.1392	0.0000	1
Mn6	0.4233	0.1407	0.0000	1
Mn7	0.4263	0.0000	0.0000	1
Si2	0.5718	0.2859	0.0000	0.52
Mn8	0.5718	0.2859	0.0000	0.48
Mn9	0.1749	0.0875	0.5000	1
Mn10	0.3405	0.1702	0.5000	1
Mn11	0.5028	0.2514	0.5000	1
Si3	0.4237	0.0837	0.5000	0.76
Mn12	0.4237	0.0837	0.5000	0.24
Mn13	0.5000	0.0000	0.5000	1
Mn14	0.3333	0.6667	0.5000	1

Table A.4
Crystal structure data of W-TiZrNi (Space-group type: no. 204 (I $m\bar{3}$), a = 14.317 Å) icosahedral quasicrystal approximant [40].

Atom	x	y	z	Occupation
Ni1	0.0000	0.0000	0.0000	1
Ni2	0.1894	0.1894	0.1894	1
Ti1	0.0000	0.1049	0.1049	1
Ti2	0.1476	0.1883	0.4020	0.4
Ti3	0.4075	0.0000	0.5000	1
Ti4	0.1965	0.0000	0.5000	0.5
Zr1	0.0000	0.3097	0.1130	1
Zr2	0.0000	0.1906	0.3115	1
Zr3	0.1476	0.1883	0.4020	0.6
Zr4	0.1965	0.0000	0.5000	0.5

Supplementary material

Supplementary material associated with this article can be found, in the online version, at 10.1016/j.ultramic.2020.113093.

References

[1] D. Shechtman, I. Blech, D. Gratias, J.W. Cahn, Metallic phase with long-range orientational order and no translational symmetry, Phys. Rev. Lett. 53 (1984) 1951–1953.
[2] D. Levine, P.J. Steinhardt, Quasicrystals: a new class of ordered structures, Phys. Rev. Lett. 53 (1984) 2477–2480, https://doi.org/10.1103/PhysRevLett.53.2477.
[3] J.-M. Dubois, Useful Quasicrystals, World Scientific, 2005.
[4] F. Zupanič, D. Wang, C. Gspan, T. Bončina, Precipitates in a quasicrystal-strengthened Al–Mn–Be–Cu alloy, Mater. Charact. 106 (2015) 93–99.
[5] K. Stan-Głowińska, Formation of quasicrystalline phases and their close approximants in cast Al–Mn base alloys modified by transition metals, Crystals 8 (2) (2018) 61.
[6] K. Stan-Głowińska, L. Lityńska-Dobrzyńska, Ł. Rogal, Influence of Fe addition on the formation of a quasicrystalline phase in bulk Al-rich Al–Mn base alloys, Mater. Character. 128 (2017) 203–208.
[7] K. Stan-Głowińska, Ł. Rogal, A. Góral, A. Wierzbicka-Miernik, J. Wojewoda-Budka, N. Schell, L. Lityńska-Dobrzyńska, Formation of a quasicrystalline phase in Al–Mn base alloys cast at intermediate cooling rates, J. Mater. Sci. 52 (13) (2017) 7794–7807.
[8] K. Stan-Głowińska, L. Lityńska-Dobrzyńska, B. Kania, J. Dutkiewicz, Ł. Rogal, W. Skuza, J. Wojewoda-Budka, M. Gordillo, J. Wiezorek, Effects of hot-compaction on the structure and properties of Al–Mn–Fe–X alloys strengthened with quasicrystalline icosahedral phase, Mater. Des. 126 (2017) 162–173.
[9] A. Singh, M. Nakamura, M. Watanabe, A. Kato, A. Tsai, Quasicrystal strengthened Mg–Zn–Y alloys by extrusion, Scripta Mater. 49 (5) (2003) 417–422.
[10] Y.K. Kim, W.T. Kim, D.H. Kim, Quasicrystal-reinforced Mg alloys, Sci. Technol. Adv. Mater. 15 (2) (2014) 024801.
[11] A. Takasaki, K. Kelton, Hydrogen storage in Ti-based quasicrystal powders produced by mechanical alloying, Int. J. Hydrog. Energy 31 (2) (2006) 183–190.
[12] T. Yadav, N. Mukhopadhyay, Quasicrystal: a low-frictional novel material, Curr. Opin. Chem. Eng. 19 (2018) 163–169.
[13] N. Rivier, Non-stick quasicrystalline coatings, J. Non-Cryst. Solids 153–154 (1993) 458–462.
[14] R.A. Dunlap, Novel Microstructures for Solids, IOP Publishing, Temple Circus, Temple Way, Bristol BS1 6HG, UK, 2018, https://doi.org/10.1088/2053-2571/aae653.
[15] International Tables for Crystallography, in: T. Hahn (Ed.), fifth ed., A: Space-Group Symmetry Springer, Dordrecht, 2005.
[16] Electron Backscatter Diffraction in Materials Science, in: A.J. Schwartz, M. Kumar, B.L. Adams (Eds.), first ed., Kluver Academic/Plenum Publishers, New York, 2000.
[17] Electron Backscatter Diffraction in Materials Science, in: A.J. Schwartz, M. Kumar, B.L. Adams, D.P. Field (Eds.), Springer US, 2009.
[18] G.C. Sneddon, P.W. Trimby, J.M. Cairney, Transmission Kikuchi diffraction in a scanning electron microscope: a review, Mater. Sci. Eng. 110 (2016) 1–12.
[19] S. Nishikawa, S. Kikuchi, The diffraction of cathode rays by calcite, Proc. Imp. Acad. 4 (1928) 475–477.
[20] L. Reimer, Scanning Electron Microscopy–Physics of Image Formation and Microanalysis, second ed., Springer Verlag, Berlin Heidelberg New York, 1998.
[21] W. Steurer, S. Deloudi, Crystallography of Quasicrystals: Concepts, Methods and Structures, Springer Series in Materials Science, Springer Berlin Heidelberg, 2009.
[22] D. Naumović, P. Aebi, L. Schlapbach, C. Beeli, K. Kunze, T. Lograsso, D. Delaney, Formation of a stable decagonal quasicrystalline Al–Pd–Mn surface layer, Phys. Rev. Lett. 87 (19) (2001) 195506. 1–4
[23] Y. Cheung, K. Chan, Y. Zhu, Characterization of the icosahedral phase in as-cast quasicrystalline Al65Cu20Fe15 alloy, Mater. Charact. 47 (2001) 299–305.
[24] G. Nolze, R. Hielscher, A. Winkelmann, Electron backscatter diffraction beyond the mainstream, Cryst. Res. Technol. 52 (1) (2016) 1600252.
[25] P.D. Asimow, C. Lin, L. Bindi, C. Ma, O. Tschauner, L.S. Hollister, P.J. Steinhardt, Shock synthesis of quasicrystals with implications for their origin in asteroid collisions, Proc. Nation. Acad. Sci. 113 (26) (2016) 7077–7081.
[26] A. Baker, M. Caputo, H. Hampikian, L. Simpson, C. Li, Icosahedral quasicrystal layer observed on λ phase in Al–Cu–Fe alloy, Mater. Sci. Appl. 08 (07) (2017) 509–520.
[27] J. Oppenheim, C. Ma, J. Hu, L. Bindi, P.J. Steinhardt, P.D. Asimow, Shock synthesis of decagonal quasicrystals, Sci. Rep. 7 (2017) 15628.
[28] I. Naglič, Z. Samardžija, K. Delijić, S. Kobe, J.-M. Dubois, B. Leskovar, B. Markoli, Metastable quasicrystals in Al–Mn alloys containing copper, magnesium and silicon, J. Mater. Sci. 52 (23) (2017) 13657–13668.
[29] F. Labib, S. Ohhashi, A.-P. Tsai, Formation and crystallographic orientation study of quasicrystal, 2/1 and 1/1 approximants in Cd–Mg–Y system using electron backscatter diffraction (EBSD), Phil. Mag. 99 (12) (2019) 1528–1550.
[30] G. Kurtuldu, K.F. Shamlaye, J.F. Löffler, Metastable quasicrystal-induced nucleation in a bulk glass-forming liquid, Proc. Natl. Acad. Sci. 115 (24) (2018) 6123–6128.
[31] L. Bindi, C. Lin, C. Ma, P.J. Steinhardt, Collisions in outer space produced an icosahedral phase in the Khatyrka meteorite never observed previously in the laboratory, Sci. Rep. 6 (1) (2016).
[32] R. Tanaka, S. Ohhashi, N. Fujita, M. Demura, A. Yamamoto, A. Kato, A. Tsai, Application of electron backscatter diffraction (EBSD) to quasicrystal-containing microstructures in the mg–Cd–Yb system, Acta Mater. 119 (2016) 193–202.
[33] S.U. Park, D. Wei, M. DeGraef, M. Shah, J. Simmons, A.O. Hero, A physics-based pattern dictionary for EBSD image segmentation, Microsc. Microanal. 19 (S2) (2013) 734–735.
[34] S. Singh, W.C. Lenthe, M.D. Graef, Many-beam dynamical scattering simulations for scanning and transmission electron microscopy modalities for 2D and 3D quasicrystals, Phil. Mag. 99 (14) (2019) 1732–1750.
[35] H. Becker, A. Leineweber, Approximate icosahedral symmetry of α-Al(Fe,Mn,Cr)Si in electron backscatter diffraction analysis of a secondary Al–Si casting alloy, Mater. Charact. 141 (2018) 406–411.
[36] G. Nolze, R. Hielscher, Orientations–perfectly colored, J. Appl. Cryst. 49 (2016) 1786–1802, https://doi.org/10.1107/S1600576716012942.
[37] W. Cao, H.Q. Ye, K.H. Kuo, A new octagonal quasicrystal and related crystalline phases in rapidly solidified Mn_4Si, Phys. Stat. Sol. (a) 107 (2) (1988) 511–519.
[38] R.C. Hudd, W.H. Taylor, The structure of Co_4Al_{13}, Acta Cryst. 15 (5) (1962) 441–442.
[39] H. Iga, M. Mihalkovič, T. Ishimasa, Approximant of dodecagonal quasicrystal formed in Mn–Si–V alloy, Phil. Mag. 91 (19–21) (2010) 2624–2633.
[40] R. Hennig, E. Majzoub, A. Carlsson, K. Kelton, C. Henley, W. Yelon, S. Misture, Structural modelling of the Ti–Zr–Ni quasicrystal, Mater. Sci. Eng. A294-A296 (2000) 361–365.
[41] L.N. Brewer, J.R. Michael, Risks of "cleaning" electron backscatter diffraction data, Microsc. Today 18 (2) (2010) 10–15.
[42] L.N. Brewer, P.G. Kotula, J.R. Michael, Multivariate statistical approach to electron backscattered diffraction. Ultramicroscopy 108 (6) (2008) 567–578, https://doi.org/10.1016/j.ultramic.2007.10.013.
[43] S.I. Wright, M.M. Nowell, R. de Kloe, P. Camus, T. Rampton, Electron imaging with an EBSD detector, Ultramicroscopy 148 (2015) 132–145, https://doi.org/10.1016/j.ultramic.2014.10.002.
[44] N. Brodusch, H. Demers, R. Gauvin, Imaging with a commercial electron backscatter diffraction (EBSD) camera in a scanning electron microscope: a review, J. Imaging 4 (7) (2018) 88, https://doi.org/10.3390/jimaging4070088.
[45] A.J. Wilkinson, D.M. Collins, Y. Zayachuk, R. Korla, A. Vilalta-Clemente, Applications of multivariate statistical methods and simulation libraries to analysis of electron backscatter diffraction and transmission Kikuchi diffraction datasets, Ultramicroscopy 196 (2019) 88–98, https://doi.org/10.1016/j.ultramic.2018.09.011.
[46] F. Bachmann, R. Hielscher, H. Schaeben, Texture analysis with MTEX–a free and open source software toolbox, Solid State Phenom. 160 (2010) 63–68.
[47] J. Qiang, Y. Wang, D. Wang, M. Kramer, C. Dong, Ti–Zr–Ni bulk quasicrystals prepared by casting, Phil. Mag. Lett. 83 (7) (2003) 467–472.
[48] B. Bauer, G. Meisterernst, J. Härtwig, T. Schenk, P. Gille, Czochralski growth and X-ray topographic characterization of decagonal AlCoNi quasicrystals, Phil. Mag. 86

(3–5) (2006) 317–322.
[49] G. Nolze, M. Jürgens, J. Olbricht, A. Winkelmann, Improving the precision of orientation measurements from technical materials via EBSD pattern matching, Acta Mater. 159 (2018) 408–415.
[50] A. Winkelmann, B.M. Jablon, V.S. Tong, C. Trager-Cowan, K.P. Mingard, Improving EBSD precision by orientation refinement with full pattern matching, J. Microsc. 277 (2) (2020) 79–92, https://doi.org/10.1111/jmi.12870.
[51] A. Winkelmann, G. Nolze, G. Cios, T. Tokarski, P. Bała, Refined calibration model for improving the orientation precision of electron backscatter diffraction maps, Materials 13 (12) (2020) 2816, https://doi.org/10.3390/ma13122816.
[52] A. Winkelmann, G. Cios, T. Tokarski, G. Nolze, R. Hielscher, T. Kozieł, EBSD orientation analysis based on experimental Kikuchi reference patterns, Acta Mater. 188 (2020) 376–385.
[53] G. Nolze, Euler angles and crystal symmetry, Cryst. Res. Technol. 50 (2) (2015) 188–201.
[54] A. Winkelmann, C. Trager-Cowan, F. Sweeney, A.P. Day, P. Parbrook, Many-beam dynamical simulation of electron backscatter diffraction patterns, Ultramicroscopy 107 (4–5) (2007) 414–421.
[55] T. Friedrich, A. Bochmann, J. Dinger, S. Teichert, Application of the pattern matching approach for EBSD calibration and orientation mapping, utilising dynamical EBSP simulations, Ultramicroscopy 184 (2018) 44–51.
[56] G. Nolze, R. Hielscher, Orientations–perfectly colored, J. Appl. Cryst. 49 (2016) 1786–1802.
[57] D.B. Litvin, The icosahedral point groups, Acta Cryst A 47 (2) (1991) 70–73.
[58] G. Nolze, A. Winkelmann, A.P. Boyle, Pattern matching approach to pseudosymmetry problems in electron backscatter diffraction, Ultramicroscopy 160 (2016) 146–154.